

Small-scale intermittency of premixed turbulent flames

Amitesh Roy^{1†‡}, Jason R. Picardo^{2¶}, Benjamin Emerson³, Tim C. Lieuwen³ and R. I. Sujith¹

¹Department of Aerospace Engineering, IIT Madras, Chennai 600 036, India

²Department of Chemical Engineering, IIT Bombay, Mumbai 400 076, India

³Daniel Guggenheim School of Aerospace Engineering, Georgia Institute of Technology, Atlanta, Georgia, 30332, USA

(Received xx; revised xx; accepted xx)

Premixed turbulent flames, encountered in power generation and propulsion engines, are an archetype of a randomly advected, self-propagating surface. While such a flame is known to exhibit large-scale intermittent flapping, the possible intermittency of its small-scale fluctuations has been largely disregarded. Here, we experimentally reveal the inner intermittency of a premixed turbulent V-flame, while clearly distinguishing this small-scale feature from large-scale outer intermittency. From temporal measurements of the fluctuations of the flame, we find a frequency spectrum that has a power-law subrange with an exponent close to -2 , which is shown to follow from Kolmogorov phenomenology. Crucially, however, the moments of the temporal increment of the flame position are found to scale anomalously, with exponents that saturate at higher-orders. This signature of small-scale inner intermittency is shown to originate from high-curvature, cusp-like structures on the flame surface, which have significance for modeling the heat release rate and other key properties of premixed turbulent flames.

Key words: turbulence, premixed flames, intermittency

1. Introduction

The dynamics of a flame in a turbulent pre-mixture of fuel and oxidant is of central importance to combustion processes and plays a key role in present-day power generation and propulsion engines. The fluctuating motion of the flame surface, which separates burned from unburned gases, is the result of a complex interplay between the propagation speed or burning velocity of the flame (which is determined by its inner chemical structure) and the multi-scale turbulent velocity field of the carrier flow (Peters 2000; Driscoll 2008; Lipatnikov & Chomiak 2010; Steinberg *et al.* 2021). The outcome is a fractal flame surface with spatial fluctuations spanning a wide range of length scales, from the size of the system down to the scale of dissipative processes (Gouldin 1987; Peters 1988; Gülder *et al.* 2000; Chatakonda *et al.* 2013). In between lies an apparently self-similar range wherein the flame fluctuations have a Fourier spectrum that varies as a power-law, which in turn follows from the inertial-range scaling of the underlying turbulent flow

† Email address for correspondence: amiteshroy94@yahoo.in

‡ Presently at the Institute for Aerospace Studies, University of Toronto, Ontario, Canada

¶ Also, Associate, International Centre for Theoretical Sciences, TIFR, India.

(Peters 1992; Peters *et al.* 2000; Chaudhuri *et al.* 2011, 2012). The statistical properties of the flame surface are widely recognized to determine crucial quantities such as the turbulent flame speed, as well as the rates of reaction, and volumetric heat generation (Kerstein *et al.* 1988; Lipatnikov & Chomiak 2002; Chaudhuri *et al.* 2012). Despite this, previous studies have almost entirely overlooked an essential property of the power-law subrange of fluctuations, namely its intermittency.

This small-scale, *inner* intermittency is fundamentally different from the well-studied *outer* intermittency of the large-scale flame motion, which is characterized by on-off flapping (Bray *et al.* 1985; Robin *et al.* 2011; Cheng & Shepherd 1987; Poinso & Veynante 2005). Although the need to recognize and study inner intermittency was emphasized by Sreenivasan (2004), the literature remains sparse (Kerstein 1991; Gülder 2007; Roy & Sujith 2021) with no experimental work, leaving a fundamental gap in our understanding of turbulent flame dynamics.

In this paper, we experimentally uncover the inner intermittency of a turbulent, CH₄-air V-flame, using high-frequency temporal measurements of the flame surface. We first clearly distinguish outer intermittency, which is apparent from the probability distribution function (PDF) of flame fluctuations ξ' , from inner intermittency, which is only revealed after a scale-by-scale analysis using temporal increments of the flame position $\delta\xi'(\tau)$. As the time interval τ decreases, the PDFs of $\delta\xi'$ exhibit increasingly non-Gaussian, flared tails indicating that the flame fluctuations contain rapid extreme events.

Next, we show how the apparently self-similar range, hitherto studied primarily in spatial wavenumber space, manifests in the temporal frequency domain: the spectrum of (ξ') has a power-law subrange, with an exponent that is shown to agree with Kolmogorov phenomenology. However, when we analyze the structure functions (moments of $\delta\xi'$) we find that they scale anomalously, with exponents that saturate at high orders. Thus, we show that the small-scale flame fluctuations violate perfect self-similarity and are, in fact, strongly intermittent. Moreover, the extreme-values of $\delta\xi'$ are found to originate from the advection of high-curvature, cusp-like structures along the flame surface. These findings have important implications for the modelling of premixed turbulent flames and suggest new directions for future work, as discussed in the concluding section of this paper.

Intermittency in *non-reacting* turbulent flows has been well studied, with comparable attention paid to both varieties. Outer intermittency is encountered in the large-scales of non-homogeneous or transitional flows (Kovaszny *et al.* 1970; Avila *et al.* 2011; Barkley *et al.* 2015), while inner intermittency is a characteristic feature of the inertial range of fully-developed, homogeneous, isotropic turbulence (Frisch 1995; Sreenivasan & Antonia 1997; Arnéodo *et al.* 2008). The intermittency of a passive and conserved scalar field, stirred by a turbulent flow, has also been studied in detail (Holzer & Siggia 1994; Tong & Warhaft 1994; Warhaft 2000), in part as a first step towards understanding the intermittency of turbulence (Shraiman & Siggia 2000; Falkovich *et al.* 2001; Falkovich & Sreenivasan 2006): the concentration fluctuations remain intermittent even when the turbulent flow is replaced by a simpler, non-intermittent, Gaussian flow (Shraiman & Siggia 2000; Tsinober 2009). Intermittent scalar fields are characterized by sharp internal fronts or ramp-cliff structures, across which the scalar experiences the largest possible fluctuation over the smallest (diffusive) spatial scale (Celani *et al.* 2000; Watanabe & Gotoh 2006).

In contrast, in the *combustion* literature, inner intermittency of scalar fields—which are neither passive nor conserved—has remained largely neglected, save for a few studies. Importantly, ramp-cliff structures have been experimentally observed in the scalar fields underlying partially premixed turbulent flames (Wang *et al.* 2007; Cai *et al.* 2009).

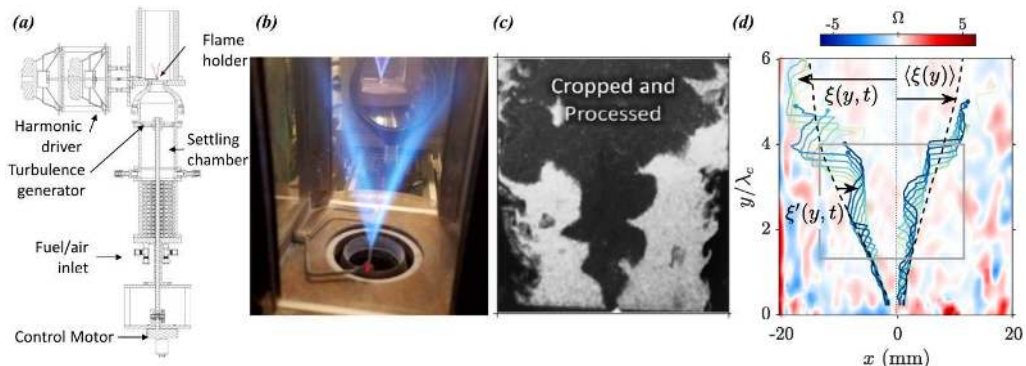


Figure 1: Turbulent V-flame facility. (a) Schematic of the combustor setup. (b) Illustrative photograph of the V-flame. (c) Representative Mie scattering snapshot depicting the flame surface. (d) Examples of the extracted instantaneous flame edge $\xi(y, t)$, along with the coordinate system. The dashed line represents the mean flame edge $\langle \xi(y) \rangle$ with respect to which the fluctuations $\xi'(y, t)$ are defined. The region highlighted by the box is used for determining the flow properties. Panels (a-c) adapted from [Humphrey *et al.* \(2018\)](#) with permission from Cambridge University Press.

Also, the extreme-value statistics of the dissipation range have been characterized, for example, through log-normal distributions of scalar dissipation, in reacting flow experiments ([Karpets & Barlow 2002](#); [Saha *et al.* 2014](#)) and simulations ([Hamlington *et al.* 2012](#); [Chaudhuri *et al.* 2017](#)). However, a clear characterization of inertial range inner intermittency in the dynamics of the flame surface is missing, and this is the focus on our work.

2. Experimental setup

2.1. Facility

Our experimental facility (figure 1a) consists of a premixed CH_4 –air V-flame stabilized on an oscillating flame holder, a typical configuration for the study of premixed flames ([Petersen & Emmons 1961](#)). The flame holder, which is an electrically heated nichrome wire, is vibrated at a frequency of $f_f = 1250$ Hz. The flow of CH_4 and air ensues out of a circular nozzle 10 mm below the flame holder, and turbulence is generated using a series of stator-rotor plates. The three-dimensional (3D) flame surface, thus obtained, is shaped like a wedge (figure 1b). We measure the fluctuations of the flame edge and the underlying velocity field within a two-dimensional plane located at the mid-section of the wedge-shaped flame surface, using TiO_2 Mie scattering and high-speed particle image velocimetry (PIV). This experimental setup has been employed previously for studying the effects of harmonic forcing and turbulence on premixed flames ([Humphrey *et al.* 2018](#); [Roy & Sujith 2019](#)).

2.2. Flame and flow characteristics

We consider two experimental flame configurations, F1 and F2, whose properties are listed in table 1. For both flames, the turbulence intensity is $u'/\bar{u}_y \approx 0.1$, where u' is the root-mean-square (r.m.s.) of the velocity fluctuations and \bar{u}_y is the mean longitudinal velocity. The Reynolds number $Re_\ell = \ell u'/\nu$ of F1 is about 700 while that of F2 is nearly

Property	Symbol	Flame F1	Flame F2
equivalence ratio	ϕ	0.97	0.91
mean longitudinal velocity	\bar{u}_y	5.1 m/s	7.33 m/s
r.m.s. velocity fluctuation	u'	0.59 m/s	0.97 m/s
turbulence intensity	u'/\bar{u}_y	0.12	0.13
kinematic viscosity	ν	$2.29 \times 10^{-6} \text{ m}^2/\text{s}$	$2.27 \times 10^{-6} \text{ m}^2/\text{s}$
flow integral length scale	ℓ	2.72 mm	6.22 mm
flow integral time scale	$\tau_\ell = \ell/u'$	$4.61 \times 10^{-3} \text{ s}$	$6.41 \times 10^{-3} \text{ s}$
Reynolds number	$Re_\ell = u'\ell/\nu$	701	2670
Kolmogorov length scale	$\eta = Re_\ell^{-3/4}\ell$	0.020 mm	0.017 mm
Kolmogorov time scale	$\tau_\eta = Re_\ell^{-1/2}\tau_\ell$	$1.75 \times 10^{-4} \text{ s}$	$1.24 \times 10^{-4} \text{ s}$
Schmidt number	Sc	0.7	0.7
Corrsin length scale	$\eta_c = Sc^{-3/4}\eta$	0.026 mm	0.022 mm
flame speed	s_L	0.37 m/s	0.34 m/s
Karlovitz number	$Ka = (\nu/Scs_L)^2\eta^{-2}$	0.20	0.32
Gibson length scale	$\ell_g = (s_L/u')^3\ell$	0.68 mm	0.27 mm

Table 1: Relevant physical properties of the two turbulent premixed flame configurations considered in this study. The laminar flame speed s_L for the two cases was obtained using Chemkin Premix calculations (Humphrey 2017), while the value of Sc for methane-air premixed flames was obtained from Tamadonfar & Gülder (2014). See the Supplemental Materials for further details.

four times larger; the dissipative Kolmogorov length (η) and time (τ_η) scales are similar though for both flames (cf. table 1).

The flame speed s_L is calculated using Chemkin Premix (Kee *et al.* 2011) with detailed chemistry simulated through the GRIMech 3.0 mechanism (Smith *et al.* 1999) at 300 K and 1 bar. The associated Karlovitz number $Ka = (\nu/Scs_L)^2\eta^{-2} \sim 0.1$, for both configurations, which implies that the flames lie within the corrugated flamelet regime, close to the boundary with the thin reaction zone regime (Peters 2000). Thus, the flame front is continuous, enabling a well-defined description of the flame edge.

Turbulent eddies can distort the flame edge and produce wrinkles or corrugations, but on scales on the order of the Gibson scale $\ell_g = (s_L/u')^3\ell \approx 0.3 \text{ mm}$ or greater. This is because smaller eddies have velocities less than the laminar flame speed s_L and so cannot distort the flame edge (Peters 2000). Further information on the properties of the flame and the flow, as well as on how these are calculated, is provided in the Supplemental Materials.

2.3. Window of interrogation

Our analysis of small-scale flame dynamics is based on measurements in a two-dimensional plane, within a sub-region of the entire domain (outlined by the grey rectangle in figure 1d). The extent of the sub-region in the longitudinal y -direction is chosen such that the flame fluctuations are not dominated by effects of flame anchoring and the oscillation of the flame holder, which is ensured for $y > \lambda_c$, where $\lambda_c = \bar{u}_y/f_f$ (notice the disappearance of the narrow-band peak from the power spectra in figure 3). Further, we disregard fluctuations at large downstream distances ($y > 4\lambda_c$) where effects of large-scale flapping become significant [discussed further below in connection with figure 2(a,b)]. The width of the sub-region in the transverse x -direction is restricted by the requirement that the measured velocity fluctuations exhibit nearly isotropic statistics.

This is verified by ensuring that the cross-correlation $\langle u'_x u'_y \rangle$ remains small (see §3 in Supplemental Materials).

Our measurements in the x – y plane give us access to the fluctuations of the flame edge in the direction normal to the mean flame edge (dashed line in figure 1d), as well as in the flow-aligned tangential direction. However, we do not have access to the fluctuations in the out-of-plane tangential direction (z -direction). We do not expect this omission to affect our key results, though, because within the sub-region of interest where the flow is approximately isotropic the only difference between these two tangential directions is the advection by the mean flow in the flow-aligned direction. We can account for this advection using Taylor’s hypothesis ($u'/\bar{u}_y \sim 0.1$) and thereby approximate the z -direction fluctuation statistics from data of the flow-aligned tangential fluctuations (Shin & Liewen 2013). This procedure is facilitated by the local homogeneity in the z -direction near the mid-section of the wedge-shaped flame surface where the measurement plane is located. In fact, many studies have carried out similar two-dimensional measurements for estimating important flame properties such as the fractal dimension of the flame surface (North & Santavicca 1990; Smallwood *et al.* 1995; Gülder *et al.* 2000).

2.4. Spatial and temporal resolution

A laser sheet of thickness 1 mm is used for Mie-scattering and PIV. The resulting images capture a region spanning $50 \times 60 \text{ mm}^2$, and the size of a pixel is $\Delta x = 0.078 \text{ mm}$. At this resolution the flame edge appears as a distinct boundary in the processed Mie-scattering images (figure 1c). The temporal frequency at which the images are obtained is $f_s = 1.25 \times 10^4 \text{ Hz}$, which based on the Nyquist theorem allows us to capture fluctuations of the interface with a maximum frequency of $f_{\text{max}} = f_s/2 = 6.25 \times 10^3 \text{ Hz}$, corresponding to a time interval of $1/f_{\text{max}} = 1.6 \times 10^{-4} \text{ s}$.

This spatio-temporal resolution is just sufficient to resolve the fluctuations of the flame edge. The thickness of the laser sheet is of the same order as the Gibson scale ℓ_g (§ 2.2), which is an estimate of the scale of the smallest turbulence-induced wrinkles on the flame edge (Peters 2000). The pixel width Δx is an order smaller than ℓ_g , and so we are able to capture the spatial undulations of the flame edge. At the Gibson scale, the inertial-range turbulent eddies have a time scale of $\ell_g/(u'(\ell_g/\ell)^{1/3}) \approx 10^{-3} \text{ s}$ (following Kolmogorov phenomenology). An even smaller convective time-scale is obtained by considering the advection of small spatial undulations along the flame surface past a fixed measurement location; using the mean longitudinal velocity as an upper estimate for the speed of convection, we obtain a time-scale of $\ell_g/\bar{u}_y \approx 10^{-4} \text{ s}$ which is approximately the same as the smallest resolved time-scale $1/f_{\text{max}}$. The ability of our measurements to capture such events will turn out to be especially important for detecting the inner intermittency of the flame dynamics (cf. § 6).

While we can analyse the flame fluctuations in detail, our resolution is insufficient to capture the dynamics of the underlying turbulent flow field. Indeed, while the pixel dimension is of the order of the Kolmogorov length ($\Delta x \approx 4\eta$), the thickness of the laser sheet is an order of magnitude larger ($\approx 50\eta$). Thus, the velocity field data obtained from our PIV images is rather coarse, and is only used to determine the r.m.s velocity fluctuation u' and the window of interrogation (cf. § 2.3) wherein the turbulence is approximately homogeneous and isotropic.

2.5. Measurement of the flame edge and its fluctuations

The instantaneous flame edge determined from TiO_2 Mie scattering (cf. figure 1c), is described by a curve in parametric form, $(x(s, t), y(s, t))$ where s is the arc-length.

(Distinct curves are obtained for the left and right flame edges.) An approximate representation that is more convenient for analysis is given by the explicit curve $x = \xi(y, t)$. These two representations are equivalent except for points where wrinkling causes the flame edge to become a locally multi-valued function of y . At such instances, we obtain a single-valued function ξ by considering the leading points of the flame edge, i.e., choosing the point with the smallest value of x for every y . This treatment is akin to viewing the flame from the side of the burnt products and making single-point measurements of its surface as it advects past various downstream stations. The curve $x = \xi(y, t)$ thus obtained is termed the leading flame edge (figure 1d). Such an approach is routinely used in studies of wrinkled flame surfaces (Zeldovich *et al.* 1985; Karpov *et al.* 1996; Chterevev *et al.* 2018) and simplifies subsequent analysis without altering our key conclusions, as discussed further in § 6 and Appendix A.

To analyse the fluctuation of the flame, which is the primary focus of this work, we first time-average to obtain the V-shaped mean flame edge $\langle \xi(y) \rangle$ (dashed line in figure 1d). The fluctuations are then defined as $\xi'(y, t) = \xi - \langle \xi \rangle$. Harnessing the transverse (x -direction) symmetry of the experimental setup, we combine the measurements of fluctuations obtained from the left and right flame edges to obtain better statistics.

Detailed information on the experimental facility, measurements, and flame edge detection is provided in the Supplemental Materials.

3. Outer and inner intermittency: two distinct forms of extreme fluctuations

Let us begin by considering the fluctuations of the flame at various distances from the flame holder. At relatively large distances, $y/\lambda_c = 5$ (where $\lambda_c = \bar{u}_y/f_f$), the flame propagation is erratic and the time series of ξ' (top panel, figure 2a) exhibits an intermittent behavior. Due to large-scale flapping, the flame undergoes abrupt excursions from the mean (bursts) at some time instances, while failing to propagate to the measurement location at other time instances (off-events). The off-events are marked by setting $\xi' = 0$, and so the corresponding normalized PDF of ξ' has a sharp peak at $\xi' = 0$ (figure 2b). Such a PDF has a high kurtosis or flatness factor, $K = \langle \xi'^4 \rangle / \langle \xi'^2 \rangle^2 = 13.51$, and is typical of large-scale outer intermittency. Now, as we move closer to the flame holder, the flame becomes well-maintained and outer intermittency is lost. Indeed, the PDF of ξ' for $y/\lambda_c = 2$ (figure 2b, see also the time series in figure 2a) has a kurtosis ($K = 3.47$) that is close to the Gaussian value of 3.

This near-Gaussian PDF of ξ' , however, veils an intermittency of a different nature, which is revealed by examining the temporal increments of the flame position $\delta\xi'(\tau) = \xi'(t + \tau) - \xi'(t)$. The normalized PDFs of this temporal structure factor, measured at $y/\lambda_c = 2$, are presented in figure 2(d) for various values of τ/τ_ℓ ($\tau_\ell = \ell/u'$ is the integral time scale). While the PDF is near-Gaussian for large τ , it develops strongly flared tails for small τ . The kurtosis for $\tau/\tau_\ell = 0.03$ is $K = 55.13$, while for $\tau/\tau_\ell = 6.67$, it is $K = 3.23$. Comparing the corresponding time series, shown in the bottom and top panels of figure 2(c) respectively, we see that $\delta\xi'(0.03\tau_\ell)$ intermittently undergoes large excursions—tens of times larger than the standard deviation—which are absent in case of $\delta\xi'(6.67\tau_\ell)$. So, while the large-scale fluctuations at $y/\lambda_c = 2$ are non-intermittent, the small-scale fluctuations exhibit extreme-value increments—a clear sign of inner intermittency.

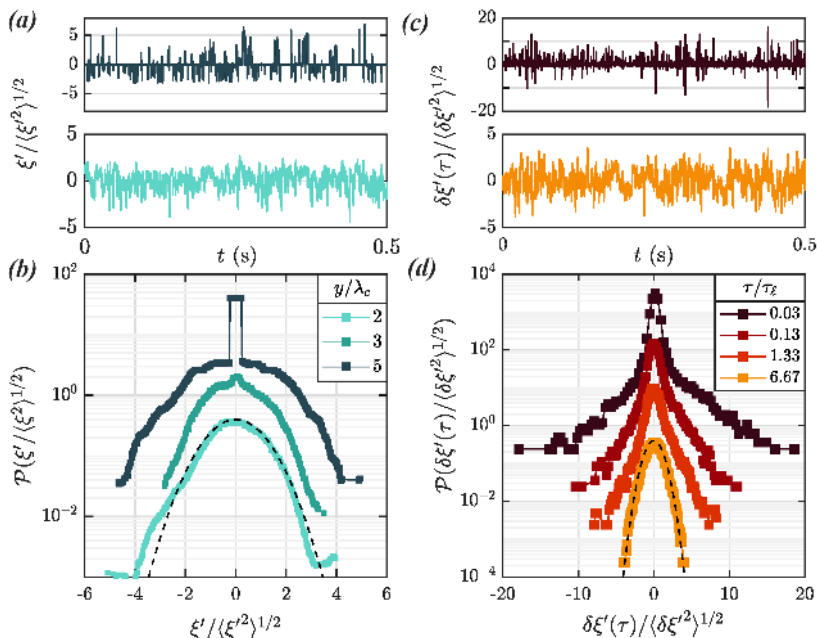


Figure 2: Distinction between outer and inner intermittency. (a) Time series of the flame fluctuations ξ' normalized by the standard deviation measured at $y = 5\lambda_c$ (top) and $y = 2\lambda_c$ (bottom). (b) PDFs of ξ' at various axial locations. (c) Time series of increments $\delta\xi'$, normalized by the standard deviation, for $\tau = 0.03\tau_\ell$ (top) and $\tau = 6.67\tau_\ell$ (bottom), measured at $y = 2\lambda_c$. (d) PDFs of the increment $\delta\xi'$ measured at $y = 2\lambda_c$ for various values of the time lag. The data set in all panels corresponds to flame F1. As explained in the text, comparing panels (b) and (d) helps to clearly distinguish large-scale outer intermittency from small-scale inner intermittency. Here, the PDFs have been shifted for clarity and the dashed lines represent $\mathcal{N}(0, 1)$ Gaussian fits.

4. Power-law scaling of the frequency spectra

Before characterizing this intermittency further, it is instructive to examine the power spectra of ξ' in frequency space, which is closely related to the variation of the second moment of $\delta\xi'$ with τ . The frequency spectra is presented in figure 3 for three axial locations. At $y/\lambda_c = 1$, we see a minor imprint of the external vibration of the flame holder, in the form of a small peak at the forcing frequency $\omega_f/\omega_\ell = 3.75$, where $\omega_\ell = 2\pi/\tau_\ell$. For $y/\lambda_c = 1.5$ and 2, there is no trace of the external forcing, and the flame's fluctuations are dominated by its response to the turbulent flow. Interestingly, for frequencies beyond ω_ℓ , a self-similar power-law is seen to emerge.

To understand the origin of this power-law, let us begin with the flame fluctuation spectra in spatial wavenumber (k) space, which has been well studied. Indeed, for a flame of finite thickness susceptible to diffusive effects [$Da \sim \mathcal{O}(1)$], in an isotropic and homogeneous turbulent flow, Kolmogorov's phenomenology (Peters 1992; Chaudhuri *et al.* 2011) leads to a spectra with a power-law behaviour,

$$\Gamma(k) \sim k^{-5/3}, \quad (4.1)$$

in the subrange $k_\ell < k < k_c$. Here $k_\ell = 2\pi/\ell$ corresponds to the large integral scale while $k_c = 2\pi/\eta_c$ is the wavenumber of the Corrsin length scale $\eta_c = Sc^{-3/4}\eta$ ($Sc = \nu/D_M$,

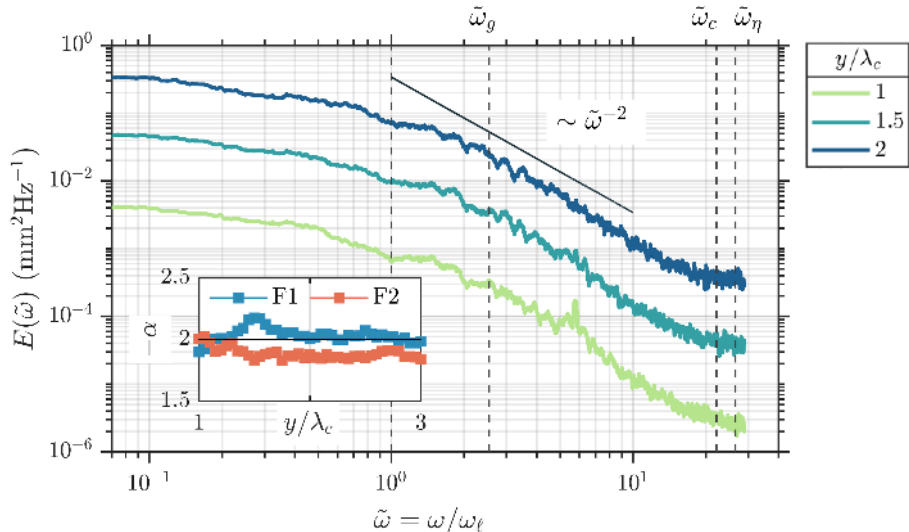


Figure 3: Temporal power spectral density $E(\tilde{\omega})$ measured at various axial locations y/λ_c , for flame F1. The power spectra varies as $E(\tilde{\omega}) \sim \tilde{\omega}^{-\alpha}$ over an intermediate range of frequencies. The estimated values of the exponent $-\alpha$ at various y/λ_c are shown in the inset for both flames F1 and F2. In both cases, the exponent is close to -2; the corresponding scaling behavior is depicted by the solid line in the main panel. The frequency corresponding to Gibson ($\tilde{\omega}_g$), Corrsin ($\tilde{\omega}_c$) and Kolmogorov ($\tilde{\omega}_\eta$) scales have been indicated by dashed lines.

where D_M is the Markstein diffusivity) after which diffusive effects within the flame become dominant. (The role of kinematic restoration is discussed below.) This subrange lies within the inertial range of the turbulent flow, $k_\ell < k < k_\eta$, where $k_\eta = 2\pi/\eta$ corresponds to the viscous Kolmogorov length η ($k_\eta > k_c$ as $Sc < 1$ for our flame). Notably, the scaling in (4.1) is the same as that for a passive scalar in the inertial-convective range (Oboukhov 1949; Corrsin 1951; Davidson 2015), which is consistent with the fact that effects due to the flame’s propagation do not play a role over this range of scales. In summary, the inertial range velocity fluctuations educe an apparently self-similar response from the flame surface, which however is cut-off by large-scale effects for $k < k_\ell$ and by diffusion within the flame for $k > k_c$.

Now, in order to translate this picture to the frequency domain, we assume that flame fluctuations with wavenumber k are most strongly influenced by a turbulent eddy of size $2\pi/k$, whose typical velocity according to inertial range scaling is $u' \sim k^{-1/3}$. We can then relate the wavenumber of flame fluctuations to the frequency as $\omega \sim ku' \sim k^{2/3}$. Then, using (4.1) and the fact that the frequency spectra $E(\omega)$ must satisfy $\int E(\omega)d\omega = \int \Gamma(k)dk$, we obtain:

$$E(\omega) \sim \omega^{-2}. \quad (4.2)$$

The exponent of the power-law subrange of the frequency spectra is presented in the inset of figure 3, and is seen to be close to this prediction of -2 for a range of axial locations, $\lambda_c < y < 3\lambda_c$. This figure also shows the frequencies ω_ℓ , ω_c and ω_η corresponding to the length scales ℓ , η_c and η , respectively. The power-law is seen to commence after ω_ℓ , as expected, and then carry on for about a decade. However, the temporal resolution of our measurements is insufficient to resolve the diffusive cutoff

and subsequent stretched-exponential decay of the spectra beyond ω_c (Peters 1992; Chaudhuri *et al.* 2011).

Figure 3 also shows the frequency ω_g , which corresponds to the Gibson length $\ell_g = (s_L/v')^3\ell$, at which the flame propagation speed becomes comparable to the turbulent velocity fluctuations. This scale could potentially cut off the power-law scaling due to kinematic restoration effects that act to smooth out turbulence-induced flame fluctuations (Lieuwen 2021). However, previous work indicates that for flames of finite thickness, this effect plays a minor role, possibly being counter-acted by thermal expansion effects, so that the power-law behavior persists until the Corrsin scale (ω_c), after which it is terminated by diffusive effects within the flame (Peters *et al.* 2000; Gülder *et al.* 2000; Shim *et al.* 2011; Chatakonda *et al.* 2013).

5. Anomalous scaling of temporal increments

Let us now return to the issue of inner intermittency and its characterization. This is best done by examining the scaling of the structure functions $S_p(\tau)$, defined as the p^{th} moment of the increment $\delta\xi'(\tau)$ (Frisch 1995; Falcon *et al.* 2007):

$$S_p(\tau; y) \equiv \langle [\delta\xi'(\tau; y)]^p \rangle = \langle [\xi'(t + \tau; y) - \xi'(t; y)]^p \rangle. \quad (5.1)$$

For the second-order structure function, which can be determined entirely from the power spectra (Davidson 2015), we have $S_2 \sim (2\pi/\tau)E(2\pi/\tau) \sim \tau$. For the p^{th} moment then, a naive expectation would be $S_p = \langle [\delta\xi']^p \rangle \sim \tau^{p/2}$; this would be true if the flame fluctuations were non-intermittent and perfectly self-similar. However the presence of extreme-value increments, evident in the flared-tail PDFs of figure 2(d), causes the higher-order moments to have increasingly large values as τ decreases. So, for intermittent fluctuations, we expect $S_p \sim \tau^{\zeta_p}$ with ζ_p becoming increasingly smaller than $p/2$ as p increases.

This is exactly what we observe in figure 4(a), which presents the values of ζ_p as a function of p , up to the sixth order, for both flame configurations, at $y = 2\lambda_c$. Figure 4(b) illustrates the corresponding power-law scaling of S_p for $\tau < \tau_\ell$. Equivalent results are obtained at other axial locations in the interval $\lambda_c < y < 3\lambda_c$, wherein the spectra exhibited a power-law exponent close to -2 (cf. Fig 3). We also estimated ζ_p using the procedure of extended self-similarity (Benzi *et al.* 1993), which takes advantage of the fact that S_p/S_2 scales as $\tau^{\zeta_p/1}$ over an extended range of τ , and obtained values nearly identical to those shown in figure 4(a). The dramatic departure of ζ_p from $p/2$, for p beyond second-order, makes evident the intensely intermittent nature of the small-scale fluctuations of the flame.

The saturation of the ζ_p exponents with increasing p , seen in figure 4(a), is reminiscent of the anomalous scaling behavior of passive scalar turbulence (Celani *et al.* 2000, 2001; Watanabe & Gotoh 2006), wherein the saturation arises due to steep ramp-cliff structures in the concentration field. The width of these structures decreases as the diffusivity is reduced, yet the amplitude of the concentration jump remains near the root-mean-square value of concentration fluctuations (Celani *et al.* 2001). In our case, figure 4(a) implies that as the diffusive Corrsin scale is reduced (keeping Da and Sc constant), the extreme-valued flame fluctuations would undergo a displacement of the order of the root-mean-square value, $\xi'_{\text{rms}} = \langle \xi'^2 \rangle^{1/2}$, in an ever-shortening time. To see this, note that in the limit of large p , $S_p^{1/p} \sim \langle \delta\xi'(\tau_\ell)^p \rangle^{1/p} (\tau/\tau_\ell)^{(\zeta_p/p)}$ is an estimate of the magnitude of extreme increments. So, given that ζ_p saturates as p increases, we see that the magnitude of extreme increments does not decrease with τ , but rather remains comparable to $\langle \delta\xi'(\tau_\ell)^p \rangle^{1/p} \sim \langle \xi'^p \rangle^{1/p} \sim \xi'_{\text{rms}}$ [ξ' has an approximately Gaussian distribution as seen

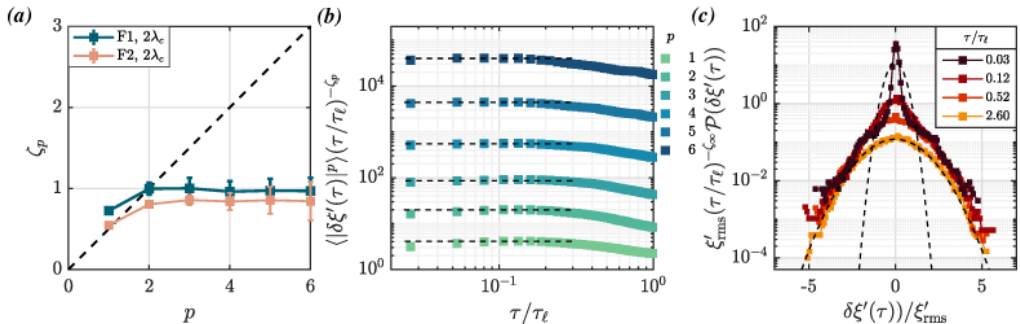


Figure 4: (a) The variation of the scaling exponents ζ_p with the order p of the structure function, for both flames at $y/\lambda_c = 2$. The dashed line indicates the non-intermittent limit of $\zeta_p = p/2$. The strong deviation of ζ_p from this limit for $p > 2$, implies that the exponents scale anomalously and that the flame fluctuations are strongly intermittent. The error bars represent the standard deviation of the measured values obtained from different time series (see § S6 in Supplemental Materials). (b) Plots of the structure functions upto order $p = 6$, compensated by the estimated scaling $\tau^{-\zeta_p}$, which illustrates their scaling behaviour (for flame F1 measured at $y = 2\lambda_c$). (c) PDFs of $\delta\xi'(\tau)$, for various values of τ , multiplied with $\xi'_{\text{rms}}(\tau/\tau_\ell)^{-\zeta_\infty}$, where ζ_∞ is the saturated value of ζ_p estimated from panel (a). The dashed lines are Gaussian fits for $\tau/\tau_\ell = 0.03$ and 2.60 . The collapse of the tails of the PDFs is striking, especially when compared with the behaviour of the Gaussian fits.

in Fig. 2(b)]. This behaviour is illustrated in Fig. 4(c), wherein the tails of the PDFs of $\delta\xi'$, for various values of τ , are seen to have the same width, and in fact collapse when the PDFs are multiplied with $\xi'_{\text{rms}}(\tau/\tau_\ell)^{-\zeta_\infty}$ [ζ_∞ is the saturated value estimated from Fig. 4(a)].

6. Origin of extreme-valued temporal increments

The extreme temporal increments implied by the saturating exponents in figure 4(a) have two possible causes: (i) rapid fluctuation events in which the flame advances and retreats very quickly, or (ii) advection of coherent spatial structures on the flame surface, such as cusps, past a fixed measurement location. The second scenario has been proposed as the cause of intermittency in temporal fluctuations of a free-surface exhibiting gravity-capillary wave turbulence (Falcon et al. 2007). For flames, and propagating surfaces in general, cusp-like features are typical (Law & Sung 2000; Zheng et al. 2017) and indeed appear quite frequently on the flame edge in our study (see figure 1c). Near such points, the flame edge typically traces out a large excursion in the transverse x direction over a short distance in the longitudinal y direction. So, when such a cusp-like structure is advected past the measurement location ($y = 2\lambda_c$ in figure 4) by the mean flow, it will register as an extreme valued increment of the flame position. The time-scale of such events is estimated in § 2.4 to be approximately 10^{-4} s, which is strikingly similar to the time-scale of the interval τ at which the PDF of $\delta\xi'(\tau)$ begins to develop strongly flared tails [see figure 2(d) wherein $\tau = 0.03\tau_\ell \approx 10^{-4}$ s]. Indeed, an examination of the temporal evolution of the flame surface in tandem with the time-trace of the temporal increment (presented in Movie M1 in the Supplemental Materials) strongly suggests that this scenario predominates and that the anomalous scaling of figure 4(a) is due to the advection of cusp-like structures along the flame edge.

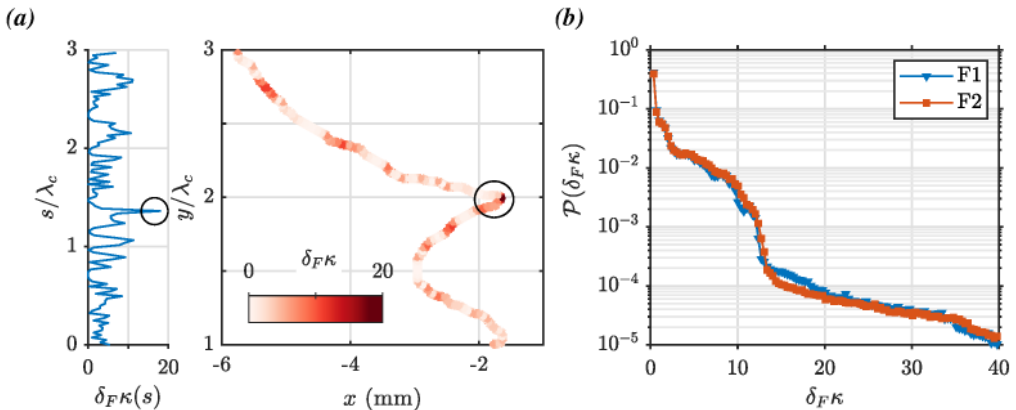


Figure 5: (a) Illustration of the variation of the curvature κ along the flame surface in the presence of a cusp-like structure. The curvature attains a large value at the cusp (right panel) and thus appears as a prominent spike in the plot of κ as a function of the arc-length s (left panel). Note that the curvature has been nondimensionalized using the flame thickness δ_F . (b) Stationary PDF of the curvature κ , shown for flames F1 and F2, exhibiting a flared positive-tail which reflects the presence of cusp-like structures on the flame surface. The PDFs are constructed by calculating the curvature along the flame edge contained within the window of interrogation (§ 2.3) and over time.

As a quantitative check, we now calculate the curvature of the flame edge and examine whether extreme values of the temporal increment $\delta\xi'$ occur simultaneously with extreme values of curvature, which would correspond to cusps. Using the parametric representation of the flame edge $(x(s, t), y(s, t))$, where s is the arc-length, the curvature κ is calculated as follows (Aris 1990):

$$\kappa(s, t) = ((\partial_{ss}x)^2 + (\partial_{ss}y)^2)^{1/2}. \quad (6.1)$$

We construct the curve $(x(s, t), y(s, t))$ using fourth-order spline interpolation based on points spaced equally along the flame edge, such that the inter-point distance ($ds = \sqrt{dx^2 + dy^2} = 0.1$ mm) is greater than the pixel size Δx . This allows us to evaluate the derivatives in (6.1) and obtain the curvature as a function of the arc-length s (see Bentkamp *et al.* 2022, for a similar calculation for material loops in turbulence). Figure 5(a) illustrates the typical variation of the curvature along the flame edge when it has a cusp-like feature: we see that the cusp corresponds to a spike in the curvature profile. Figure 5(b) presents the stationary PDF of curvature values sampled by the flame edge, within the interrogation window (box in figure 1d) and over time. The heavy-tail of the distribution is a consequence of the extreme curvature values associated with cusp-like features of the flame surface.

Having calculated the flame curvature, we next examine its correlation with the temporal increment of the flame fluctuations. Each measurement of the increment $\delta\xi'(\tau; y^*)$ is associated with curvature values at two time instances, $\kappa(t; s_1)$ and $\kappa(t + \tau; s_2)$, where the values of s_1 and s_2 are such that $y(s_1) = y(s_2) = y^*$ corresponds to the measurement location. Note that there will be more than one value of s_1 , or s_2 , when the flame edge becomes locally multi-valued. We consider the maximum of these curvature values $\max\{\kappa(t), \kappa(t + \tau)\}$ and depict its joint probability distribution function with the magnitude of the associated increment of the flame position $|\delta\xi'(\tau)|$ in figure 6, for various

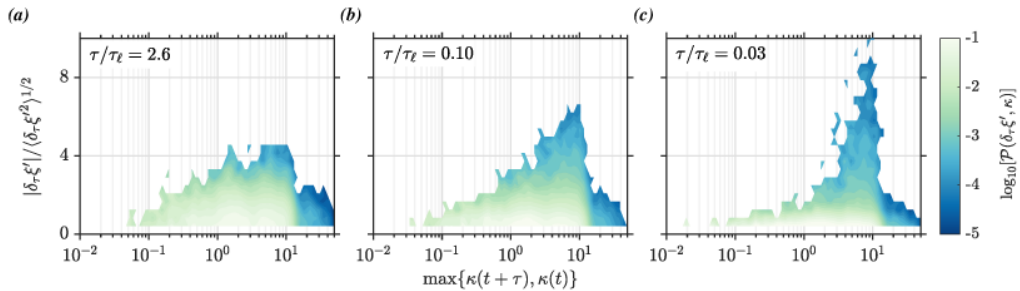


Figure 6: Pseudo-color plot of the joint probability distribution function of the increment $\delta\xi'(\tau; y)$ and the maximum of the flame curvature values at times instances t and $t + \tau$, as measured at $y = 2\lambda_c$. The three panels correspond to different values of the time increment τ/τ_ℓ : (a) 2.67, (b) 0.10 and (b) 0.03. The extreme-valued increments which appear as τ decreases show a clear correlation with extreme values of the curvature. These results correspond to flame F1 and are measured at $y = 2\lambda_c$; similar results are obtained for flame F2 and for other measurement locations within $1 < y/\lambda_c < 3$. The colored contours correspond to the the logarithm of the joint PDF.

time intervals τ . Clearly, the extreme-values of the temporal increment which arise as τ decreases are strongly correlated with extreme-values of the flame curvature. This is entirely consistent with our observation that large and rapid temporal fluctuations of the flame position are registered when cusp-like structures are advected past the measurement location.

Cusp-like features and wrinkling in general can cause the flame edge to become a locally multi-valued function of y . This fact is accounted for in the calculation of curvature $\kappa(s, t)$ which is based on the arc-length parameterization, but not in the measurement of increments $\delta\xi'$ which is based on the single-valued leading edge $\xi(y, t)$. This raises the concern that multi-valued regions of the flame edge may appear as artificially abrupt variations in $\xi(y, t)$ which would in turn produce spurious large values of the increment. In Appendix A, we carry out two checks which show that our detection of inner intermittency is not an artifact of the treatment of the flame edge. First, we modify how we obtain the single-valued function $\xi(y, t)$: instead of taking the points closest to the y axis, we now locally average the flame edge in regions where it is multi-valued. This procedure would smooth out artificially abrupt variations in $\xi(y, t)$. Second, we retain the leading edge profile, but eliminate all data points where the flame edge is multi-valued, i.e., we only calculate increments when $\xi(y)$ is single valued at both times, t and $t + \tau$. For both cases, we find that anomalous scaling persists, which shows that the inner intermittency detected in this study is a genuine feature of the flame dynamics.

7. Concluding Remarks

To summarize, we have seen that a well-maintained flame surface, devoid of large-scale bursts associated with outer-intermittency, contains a subrange of scales wherein the flame surface merely responds to the fluctuations of the incident turbulent flow and exhibits power-law scaling that is entirely determined by the inertial-range scaling of the flow. However, this apparent simplicity comes along with a caveat, which is the key result of our work: the flame fluctuations are intensely intermittent with structure functions that exhibit strongly anomalous scaling. The associated extreme events, which originate from cusp-like structures that are advected along the flame edge, have important

implications for the modeling of turbulent premixed flames. For example, cusps with their extremely large values of flame curvature will affect the mean turbulent flame speed (Law 2010; Humphrey *et al.* 2018; Dave & Chaudhuri 2020). Furthermore, closure models of turbulent flame speeds and volumetric heat release rate, which depend on the fractal dimension of the flame surface, assume perfect self-similarity and so may be improved by accounting for inner intermittency (Charlette *et al.* 2002; Gülder 2007; Roy & Sujith 2021).

It is intriguing to consider how the cusp-like features on the flame surface are related to the small-scale structures, such as ramp-cliffs, of the underlying scalar fields. While ramp-cliff structures have been observed in DNS simulations of premixed combustion (Wang *et al.* 2007; Cai *et al.* 2009), their connection to intermittent fluctuations of the flame surface is unknown. More generally, the question of how the statistics of the flame surface are connected to that of the reacting scalar fields of combustion, possibly via a flame indicator function (Thiesset *et al.* 2016), deserves further study especially in light of the extensive literature on the turbulent transport of conserved scalars (Warhaft 2000; Falkovich & Sreenivasan 2006); one would require simultaneous high-resolution measurements of the flame surface and the scalar fields, which while beyond our current scope is an important task for future work.

It is also interesting to note that the equation for the propagation of a thin premixed flame resembles the Kardar-Parisi-Zhang (KPZ) equation (Kerstein *et al.* 1988; Kardar *et al.* 1986) [in turn closely related to the Burgers equation (Bec & Khanin 2007)], whose dynamics in the presence of additive noise is well-studied (Verma 2000). However, a crucial difference arises due to the advection of the flame by the turbulent flow, which, if modeled as a random flow, appears as multiplicative noise. This results in fundamentally distinct dynamics (Yakhot 1988; Kerstein *et al.* 1988), for example, the propagating flame attains a statistically stationary mean speed in contrast to the power-law growth predicted by the KPZ equation with additive noise. Thus, in light of the present results, it would be interesting to explore the intermittent properties of the KPZ equation with multiplicative and spatio-temporally correlated noise.

Finally, while we have focused on temporal measurements, the cusp-like structures of the flame surface will certainly give rise to inner intermittency in space, so that spatial structure functions obtained from a flame edge profile at a single snapshot in time should scale anomalously. Establishing this experimentally would require a very large flame in order to capture the required range of spatial scales, a challenge that will hopefully be taken up in the future. Other important questions raised by our work include how the inner intermittency of the self-similar range relates to the extreme-value statistics of the sub-diffusive dissipative scales (Hamlington *et al.* 2012; Chaudhuri *et al.* 2017), and whether the scaling exponents for a premixed flame are universal, as they seem to be for a passive scalar (Watanabe & Gotoh 2006).

Acknowledgements

This research was conceptualized following a visit to the International Centre for Theoretical Sciences (ICTS), India for participating in the program - Turbulence: From Angstroms to light years (Code: ICTS/Prog-taly2018/01). The authors thank Luke Humphrey (Georgia Tech) for sharing his experimental data. The authors benefited from discussions at the Inter Group Meetings held at IIT Madras, ICTS Bangalore, and IIT Bombay. A.R. and J.R.P. also thank Samriddhi Sankar Ray (ICTS) and Jeremie Bec (MINES ParisTech) for insightful discussions and comments.

A.R. is grateful for the HTRA Ph.D. fellowship from MHRD, India. J.R.P. is thankful

for financial support from the IIT Bombay IRCC Seed Grant and from the DST-SERB grant (SRG/2021/001185). T.C.L. gratefully acknowledges the support received from Air Force Office of Scientific Research (Contract no. FA 9550-20-1-0215), contract monitor Dr. Chiping Li. R.I.S. gratefully acknowledges funding from the Institute of Excellence Grant (SB/2021/0845/AE/MHRD/002696) and the J. C. Bose Fellowship (No. JCB/2018/000034/SSC).

Appendix A. Anomalous scaling persists after smoothing or eliminating multi-valued flame wrinkles

Wrinkling of the flame in turbulence causes the flame edge $(x(s), y(s))$ to become locally multi-valued, so that there will be multiple values of $x(s)$ for each $y(s)$. In the main text, such multi-valued regions of the flame edge are converted to a single-valued function of y —the leading flame edge—by choosing the value of x with the smallest magnitude. While this treatment allows for a straightforward definition of the flame fluctuation and its temporal increment, it does introduce the possibility of multi-valued folds in the flame edge $(x(s), y(s))$ being registered as artificially abrupt variations in the leading flame edge $\xi(y)$. This could in turn produce artificial large increments when these folds are advected past a fixed longitudinal measurement location. Here, we carry out two checks which are designed to reduce or eliminate the effect of such multi-valued folds on the statistics of the flame increment; if the anomalous scaling behaviour persists then we can be confident that it is a genuine feature of the flame dynamics.

First, rather than using the leading flame edge, we construct a locally averaged flame edge $\tilde{\xi}(y, t)$, where for each value of y we set $\tilde{\xi}$ to be equal to the average of all the corresponding values of x (mathematical definitions for both flame edges is given in the Supplemental Materials). Any multi-valued folds which appear as abrupt variations in $\xi(y, t)$ will be significantly smoothed out in $\tilde{\xi}(y, t)$. Of course, where the flame is single valued, ξ and $\tilde{\xi}$ will be identical. We then define the fluctuations and the increment as $\tilde{\xi}'(y, t) = \tilde{\xi} - \langle \tilde{\xi} \rangle$ and $\delta\tilde{\xi}'(\tau) = \tilde{\xi}'(t + \tau) - \tilde{\xi}'(t)$ respectively, and determine the scaling exponents ζ_p just as we do in the main text. The results, presented in figure 7(a), show strongly intermittent behaviour similar to that seen in figure 4(a).

As a second check, we return to the leading flame edge, but now entirely eliminate any points where the flame edge is multi-valued from the calculation of the scaling exponents. For this, we first flag any time instant at which the flame edge $(x(s), y(s))$ is multi-valued. Then, while calculating the increments $\delta\xi' = \xi'(t + \tau) - \xi'(t)$, we check to see if either of the two data points are flagged (i.e. if the flame edge is multi-valued at either time instant), and if so we discard the corresponding increment value. The filtered set of data values thus obtained correspond to increments $\delta\xi'(\tau)$ such that the flame edge is single-valued at both t and $t + \tau$. This procedure will entirely eliminate any large-valued increments due to folds in the flame edge being advected past the measurement location y . The scaling exponents obtained from this filtered data set are compared with those obtained from the unfiltered data in figure 7(b). We see that the strongly anomalous scaling behaviour persists, although the loss of data due to filtering enlarges the error bars especially for large values of the order p .

Taken together, these two checks demonstrate that the inner intermittency of the flame fluctuations detected in this work is *not* an artifact of representing the edge by a single-valued function. As shown in § 6, the extreme-valued increments arise from the advection of cusp-like structures past the measurement location. These cusp-like features correspond to genuine sharp variations of the flame edge, and so representing them by the single-valued leading edge does not introduce artificial abrupt variations even when

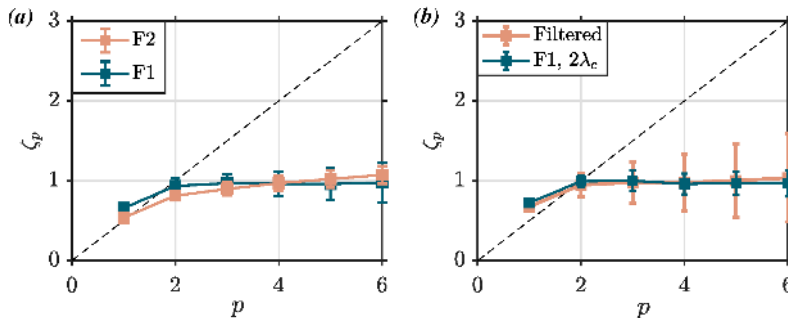


Figure 7: Anomalous scaling of the exponents of the structure function, calculated after implementing two procedures that are designed to reduce or eliminate any artificial large increments in the flame position that arise from multi-valued folds or wrinkles being described by the single-valued leading flame edge. First, for panel (a), we use the locally averaged flame edge profile, which averages over multi-valued regions of the flame thereby providing a much smoother representation of multi-valued folds when compared to the leading edge. Second, for panel (b), we use a filtered data set of increments of the leading edge, obtained by removing any increment value that is calculated using time instants when the flame is multi-valued. The filtered data set is therefore entirely free from the influence of multi-valued regions of the flame, and the exponents of the corresponding structure functions are compared with those of the full data set, for the case of flame F1. Clearly, the anomalous scaling behavior persists for the locally averaged flame edge, as well as for the filtered data (which however has enlarged error bars due to a reduction of data points).

the cusps are multi-valued. So, though the precise values of the flame fluctuation and its increment depends on the manner in which the flame edge is described, their statistical features including anomalous scaling are qualitatively alike.

REFERENCES

- ARIS, R. 1990 *Vectors, tensors, and the basic equations of fluid mechanics*. Dover Publications Inc.
- ARNÉODO, A., BENZI, R., BERG, J., BIFERALE, L., BODENSCHATZ, E., BUSSE, A., CALZAVARINI, E., CASTAING, B., CENCINI, M., CHEVILLARD, L. & OTHERS 2008 Universal intermittent properties of particle trajectories in highly turbulent flows. *Phys. Rev. Lett.* **100** (25), 254504.
- AVILA, K., MOXEY, D., DE LOZAR, A., AVILA, M., BARKLEY, D. & HOF, B. 2011 The onset of turbulence in pipe flow. *Sci.* **333** (6039), 192–196.
- BARKLEY, D., SONG, B., MUKUND, V., LEMOULT, G., AVILA, M. & HOF, B. 2015 The rise of fully turbulent flow. *Nature* **526** (7574), 550–553.
- BEC, J. & KHANIN, K. 2007 Burgers turbulence. *Phys. Rep.* **447** (1), 1–66.
- BENTKAMP, L., DRIVAS, T. D., LALESCU, C. C. & WILCZEK, M. 2022 The statistical geometry of material loops in turbulence. *Nature Comm.* **13** (1), 1–10.
- BENZI, R., CILIBERTO, S., TRIPPICIONE, R., BAUDET, C., MASSAIOLI, F. & SUCCI, S. 1993 Extended self-similarity in turbulent flows. *Phys. Rev. E* **48** (1), R29.
- BRAY, K. N. C., LIBBY, P. A. & MOSS, J. B. 1985 Unified modeling approach for premixed turbulent combustion—Part I: General formulation. *Combust. Flame* **61** (1), 87–102.
- CAI, J., WANG, D., TONG, C., BARLOW, R. S. & KARPETIS, A. N. 2009 Investigation of subgrid-scale mixing of mixture fraction and temperature in turbulent partially premixed flames. *Proc. Combust. Inst.* **32** (1), 1517–1525.

- CELANI, A., LANOTTE, A., MAZZINO, A. & VERGASSOLA, M. 2000 Universality and saturation of intermittency in passive scalar turbulence. *Phys. Rev. Lett.* **84** (11), 2385.
- CELANI, A., LANOTTE, A., MAZZINO, A. & VERGASSOLA, M. 2001 Fronts in passive scalar turbulence. *Phys. Fluids* **13** (6), 1768–1783.
- CHARLETTE, F., MENEVEAU, C. & VEYNANTE, D. 2002 A power-law flame wrinkling model for les of premixed turbulent combustion part I: non-dynamic formulation and initial tests. *Combust. Flame* **131** (1-2), 159–180.
- CHATAKONDA, O., HAWKES, E. R., ASPDEN, A. J., KERSTEIN, A. R., KOLLA, H. & CHEN, J. H. 2013 On the fractal characteristics of low Damköhler number flames. *Combust. Flame* **160** (11), 2422–2433.
- CHAUDHURI, S., AKKERMAN, V. & LAW, C. K. 2011 Spectral formulation of turbulent flame speed with consideration of hydrodynamic instability. *Phys. Rev. E* **84** (2), 026322.
- CHAUDHURI, S., KOLLA, H., DAVE, H. L., HAWKES, E. R., CHEN, J. H. & LAW, C. K. 2017 Flame thickness and conditional scalar dissipation rate in a premixed temporal turbulent reacting jet. *Combust. Flame* **184**, 273–285.
- CHAUDHURI, S., WU, F., ZHU, D. & LAW, C. K. 2012 Flame speed and self-similar propagation of expanding turbulent premixed flames. *Phys. Rev. Lett.* **108** (4), 044503.
- CHENG, R. K. & SHEPHERD, I. G. 1987 Intermittency and conditional velocities in premixed conical turbulent flames. *Combust. Sci. Tech.* **52** (4-6), 353–375.
- CHTEREV, I., EMERSON, B. & LIEUWEN, T. 2018 Velocity and stretch characteristics at the leading edge of an aerodynamically stabilized flame. *Combust. Flame* **193**, 92–111.
- CORRSIN, S. 1951 On the spectrum of isotropic temperature fluctuations in an isotropic turbulence. *J. Appl. Phys.* **22** (4), 469–473.
- DAVE, H. L. & CHAUDHURI, S. 2020 Evolution of local flame displacement speeds in turbulence. *J. Fluid Mech.* **884**.
- DAVIDSON, P. A. 2015 *Turbulence: An introduction for scientists and engineers*. Oxford university press.
- DRISCOLL, J. F. 2008 Turbulent premixed combustion: Flamelet structure and its effect on turbulent burning velocities. *Prog. Energy Combust. Sci.* **34** (1), 91–134.
- FALCON, E., FAUVE, S. & LAROCHE, C. 2007 Observation of intermittency in wave turbulence. *Phy. Rev. Lett.* **98** (15), 154501.
- FALKOVICH, G., GAWĘDZKI, K. & VERGASSOLA, M. 2001 Particles and fields in fluid turbulence. *Rev. Mod. Phys.* **73**, 913–975.
- FALKOVICH, G. & SREENIVASAN, K. 2006 Lessons from hydrodynamic turbulence. *Phys. Today* **59** (4), 43.
- FRISCH, U. 1995 *Turbulence: The legacy of A N Kolmogorov*. Cambridge university press.
- GOULDIN, F. C. 1987 An application of fractals to modeling premixed turbulent flames. *Combust. Flame* **68** (3), 249–266.
- GÜLDER, ÖL, SMALLWOOD, GREGORY J, WONG, ROGER, SNELLING, DR, SMITH, ROGER, DESCHAMPS, BM & SAUTET, J-C 2000 Flame front surface characteristics in turbulent premixed propane/air combustion. *Combust. Flame* **120** (4), 407–416.
- GÜLDER, Ö. L. 2007 Contribution of small scale turbulence to burning velocity of flamelets in the thin reaction zone regime. *Proc. Combust. Inst.* **31** (1), 1369–1375.
- HAMLINGTON, P. E., POLUDNENKO, A. Y. & ORAN, E. S. 2012 Intermittency in premixed turbulent reacting flows. *Phys. Fluids* **24** (7), 075111.
- HOLZER, M. & SIGGIA, E. D. 1994 Turbulent mixing of a passive scalar. *Phys. Fluids* **6** (5), 1820–1837.
- HUMPHREY, L. 2017 Ensemble-averaged dynamics of premixed, turbulent, harmonically excited flames. PhD thesis, Georgia Institute of Technology.
- HUMPHREY, L. J., EMERSON, B. & LIEUWEN, T. C. 2018 Premixed turbulent flame speed in an oscillating disturbance field. *J. Fluid Mech.* **835**, 102–130.
- KARDAR, M., PARISI, G. & ZHANG, Y.-C. 1986 Dynamic scaling of growing interfaces. *Phys. Rev. Lett.* **56**, 889–892.
- KARPETIS, A. N. & BARLOW, R. S. 2002 Measurements of scalar dissipation in a turbulent piloted methane/air jet flame. *Proc. Combust. Inst.* **29** (2), 1929–1936.

- KARPOV, V., LIPATNIKOV, A. & OTHERS 1996 A test of an engineering model of premixed turbulent combustion. In *Symposium (Int.) Combust.*, , vol. 26, pp. 249–257. Elsevier.
- KEE, R. J. & OTHERS 2011 Chemkin 10112, Reaction design: San Diego.
- KERSTEIN, A. R. 1991 Fractal dimension of propagating interfaces in turbulence. *Phys. Rev. A* **44** (6), 3633.
- KERSTEIN, A. R., ASHURST, W. T. & WILLIAMS, F. A. 1988 Field equation for interface propagation in an unsteady homogeneous flow field. *Phys. Rev. A* **37** (7), 2728.
- KOVASZNAV, L. S. G., KIBENS, V. & BLACKWELDER, R. F. 1970 Large-scale motion in the intermittent region of a turbulent boundary layer. *J. Fluid Mech.* **41** (2), 283–325.
- LAW, C. K. 2010 *Combustion physics*. Cambridge university press.
- LAW, C. K. & SUNG, C. J. 2000 Structure, aerodynamics, and geometry of premixed flamelets. *Prog. Energy Combust. Sci.* **26** (4), 459–505.
- LIEUWEN, T. C. 2021 *Unsteady combustor physics*. Cambridge University Press.
- LIPATNIKOV, A. N. & CHOMIAK, J. 2002 Turbulent flame speed and thickness: phenomenology, evaluation, and application in multi-dimensional simulations. *Prog. Energy Combust. Sci.* **28** (1), 1–74.
- LIPATNIKOV, A. N. & CHOMIAK, J. 2010 Effects of premixed flames on turbulence and turbulent scalar transport. *Prog. Energy Combust. Sci.* **36** (1), 1–102.
- NORTH, G. L. & SANTAVICCA, D. A. 1990 The fractal nature of premixed turbulent flames. *Combust. Sci. Tech.* **72** (4-6), 215–232.
- OBOUKHOV, A. M. 1949 Structure of the temperature field in turbulent flows. *Isv. Geogr. Geophys. Ser.* **13**, 58–69.
- PETERS, N. 1988 Laminar flamelet concepts in turbulent combustion. In *Symp. Int. Comb.*, , vol. 21, pp. 1231–1250. Elsevier.
- PETERS, N. 1992 A spectral closure for premixed turbulent combustion in the flamelet regime. *J. Fluid Mech.* **242**, 611–629.
- PETERS, N. 2000 *Turbulent combustion*. Cambridge University Press.
- PETERS, N., WENZEL, H. & WILLIAMS, F. A. 2000 Modification of the turbulent burning velocity by gas expansion. *Proc. Combust. Inst.* **28** (1), 235–243.
- PETERSEN, R. E. & EMMONS, H. W. 1961 Stability of laminar flames. *Phys. Fluids* **4** (4), 456–464.
- POINSOT, T. & VEYNANTE, D. 2005 *Theoretical and numerical combustion*. RT Edwards, Inc.
- ROBIN, V., MURA, A. & CHAMPION, M. 2011 Direct and indirect thermal expansion effects in turbulent premixed flames. *J. Fluid Mech.* **689**, 149–182.
- ROY, A. & SUJITH, R. I. 2019 Nonlinear flame response dependencies of a v-flame subjected to harmonic forcing and turbulence. *Combust. Flame* **207**, 101–119.
- ROY, A. & SUJITH, R. I. 2021 Fractal dimension of premixed flames in intermittent turbulence. *Combust. Flame* **226**, 412 – 418.
- SAHA, A., CHAUDHURI, S. & LAW, C. K. 2014 Flame surface statistics of constant-pressure turbulent expanding premixed flames. *Phys. Fluids* **26** (4), 045109.
- SHIM, Y., TANAKA, S., TANAHASHI, M. & MIYAUCHI, T. 2011 Local structure and fractal characteristics of H₂–air turbulent premixed flame. *Proc. Combust. Inst.* **33** (1), 1455–1462.
- SHIN, DONG-HYUK & LIEUWEN, TIMOTHY 2013 Flame wrinkle destruction processes in harmonically forced, turbulent premixed flames. *J. Fluid Mech.* **721**, 484–513.
- SHRAIMAN, B. I. & SIGGIA, E. D. 2000 Scalar turbulence. *Nature* **405** (6787), 639–646.
- SMALLWOOD, G. J., GÜLDER, Ö. L., SNELLING, D. R., DESCHAMPS, B. M. & GÖKALP, I. 1995 Characterization of flame front surfaces in turbulent premixed methane/air combustion. *Combust. Flame* **101** (4), 461–470.
- SMITH, G. P. & OTHERS 1999 GRI-Mech 3.0 chemical mechanism.
- SREENIVASAN, K. R. 2004 Possible effects of small-scale intermittency in turbulent reacting flows. *Flow, Turb. Combust.* **72** (2-4), 115–131.
- SREENIVASAN, K. R. & ANTONIA, R. A. 1997 The phenomenology of small-scale turbulence. *Ann. Rev. Fluid Mech.* **29** (1), 435–472.
- STEINBERG, A. M., HAMLINGTON, P. E. & ZHAO, X. 2021 Structure and dynamics of highly turbulent premixed combustion. *Prog. Energy Combust. Sci.* **85**, 100900.

- TAMADONFAR, P. & GÜLDER, Ö. L. 2014 Flame brush characteristics and burning velocities of premixed turbulent methane/air bunsen flames. *Combust. Flame* **161** (12), 3154–3165.
- THIESSET, F., MAURICE, G., HALTER, F., MAZELLIER, N., CHAUVEAU, C. & GÖKALP, I. 2016 Geometrical properties of turbulent premixed flames and other corrugated interfaces. *Phys. Rev. E* **93** (1), 013116.
- TONG, C. & WARHAFT, Z. 1994 On passive scalar derivative statistics in grid turbulence. *Phys. Fluids* **6** (6), 2165–2176.
- TSINOBER, A. 2009 *An informal conceptual introduction to turbulence*. New York, USA: Springer.
- VERMA, M. K. 2000 Intermittency exponents and energy spectrum of the Burgers and KPZ equations with correlated noise. *Phys. A* **277**, 359–388.
- WANG, D., TONG, C., BARLOW, R. S. & KARPETIS, A. N. 2007 Experimental study of scalar filtered mass density function in turbulent partially premixed flames. *Proc. Combust. Inst.* **31** (1), 1533–1541.
- WARHAFT, Z. 2000 Passive scalars in turbulent flows. *Ann. Rev. Fluid Mech.* **32** (1), 203–240.
- WATANABE, T. & GOTOH, T. 2006 Intermittency in passive scalar turbulence under the uniform mean scalar gradient. *Phys. Fluids* **18** (5), 058105.
- YAKHOT, V. 1988 Propagation velocity of premixed turbulent flames. *Combust. Sci. Tech.* **60** (1–3), 191–214.
- ZELDOVICH, I. A., BARENBLATT, G. I., LIBROVICH, V. B. & MAKHVILADZE, G. M. 1985 *Mathematical theory of combustion and explosions*. Consultants Bureau, New York, NY.
- ZHENG, T., YOU, J. & YANG, Y. 2017 Principal curvatures and area ratio of propagating surfaces in isotropic turbulence. *Phys. Rev. Fluids* **2**, 103201.